Solar Phys (2013) 284:105–127
DOI 10.1007/s11207-013-0224-9



# Comparison of Helicity Signs in Interplanetary CMEs and Their Solar Source Regions

**K.-S. Cho · S.-H. Park · K. Marubashi · N. Gopalswamy · S. Akiyama · S. Yashiro · R.-S. Kim · E.-K. Lim**

Received: 6 April 2012 / Accepted: 5 January 2013 / Published online: 7 February 2013


**Abstract** If all coronal mass ejections (CMEs) have flux ropes, then the CMEs should keep their helicity signs from the Sun to the Earth according to the helicity conservation principle. This study presents an attempt to answer the question from the Coordinated Data Analysis Workshop (CDAW), "Do all CMEs have flux ropes?", by using a qualitative helicity sign comparison between interplanetary CMEs (ICMEs) and their CME source regions. For this, we select 34 CME–ICME pairs whose source active regions (ARs) have continuous SOHO/MDI magnetogram data covering more than 24 hr without data gap during the passage of the ARs near the solar disk center. The helicity signs in the ARs are determined by estimation of cumulative magnetic helicity injected through the photosphere in the entire source ARs. The helicity signs in the ICMEs are estimated by applying the cylinder model developed by Marubashi (*Adv. Space. Res.*, **26**, 55, 2000) to 16 second resolution magnetic field data from the MAG instrument onboard the ACE spacecraft. It is found that 30 out of 34 events (88 %) are helicity sign-consistent events, while four events (12 %) are sign-inconsistent. Through a detailed investigation of the source ARs of the four sign-inconsistent events, we find that those events can be explained by the local helicity sign opposite to that of the entire AR helicity (28 July 2000 ICME), incorrectly reported solar source region in the CDAW list (20 May 2005 ICME), or the helicity sign of the pre-existing coronal magnetic field (13 October 2000 and 20 November 2003 ICMEs). We conclude that the helicity

Flux-Rope Structure of Coronal Mass Ejections
Guest Editors: N. Gopalswamy, T. Nieves-Chinchilla, M. Hidalgo, J. Zhang, and P. Riley

K.-S. Cho (✉) · S.-H. Park · K. Marubashi
Korea Astronomy and Space Science Institute, Daejeon 305-348, Republic of Korea
e-mail: kscho@kasi.re.kr

K.-S. Cho · N. Gopalswamy · S. Akiyama · S. Yashiro · R.-S. Kim
NASA Goddard Space Flight Center, Greenbelt, MD 20771, USA

K.-S. Cho · S. Akiyama · S. Yashiro · R.-S. Kim
Department of Physics, The Catholic University of America, Washington, DC 20064, USA

E.-K. Lim
Big Bear Solar Observatory, New Jersey Institute of Technology, Newark, CA, USA

signs of the ICMEs are quite consistent with those of the injected helicities in the AR regions from where the CMEs erupted.

**Keywords** Coronal mass ejections · Magnetic cloud · Photospheric helicity · Solar surface magnetic field · Interplanetary magnetic field

## 1. Introduction

Coronal mass ejections (CMEs) are one of the means by which the Sun ejects plasma and magnetic field into interplanetary space. When CMEs are detected near the Earth, they are known as interplanetary CMEs (ICMEs). ICMEs are further classified into magnetic clouds (MC) and complex ejecta (EJ) depending on the observed magnetic structure. MCs exhibit a smooth rotation of magnetic field vector, while EJs do not show a significant rotation signature (*e.g.* Burlaga *et al.*, 1981). It is still not clear whether MC and EJ have intrinsically different structure or the observed structure is due to different propagation of the ejecta relative to the observing spacecraft. The main purpose of the Coordinated Data Analysis Workshop (CDAW) this article results from is to answer the question: "Do all CMEs have flux ropes?" There are two different views. One view is that some CMEs have inherently non-flux rope structure (Gosling *et al.*, 1990; Jacobs *et al.*, 2009), and the other view is that all the CMEs have flux ropes but sometimes they are not detected as flux ropes since a magnetic cloud observed far from its apex (nose) may not exhibit a clear flux rope structure (Gopalswamy, 2006; Kim *et al.*, 2013). For example, Chen *et al.* (1997) compared LASCO C2 and C3 CME images with a magnetic flux rope model, and concluded that the dynamics and morphology of the observed CME on 13 April 1997 were consistent with those of the three-dimensional (3D) MHD flux rope model developed by Chen (1996).

Magnetic helicity quantifies the signed amount of twists, kinks, and inter-linkages of the magnetic field lines in a given magnetic field system (Berger and Field, 1984). Magnetic helicity is an approximately conserved quantity in resistive MHD with low resistivity (Berger, 1984) – this is the 'helicity conservation principle'. Therefore, an ICME is expected to carry the same amount of helicity as its corresponding CME from the solar source region, and the helicity sign of the ICME should be consistent with that of the solar source region. Several attempts have been made to match the helicity sign of ICMEs with that inferred from the morphological features of their source active region such as sunspot whorls, filament barbs, sigmoids, and flare ribbons (*e.g.* Ali *et al.*, 2007; Démoulin, 2008). However, the helicity sign of the solar source region was not always found to agree with that of the ICME (Leamon *et al.*, 2004). These observational features have been commonly used for qualitative comparison of helicity signs of CMEs and ICMEs. In this study, we use the helicity signs of solar source regions and ICMEs that are determined in the following ways:

i) measurement of the rate of the helicity transfer into the corona across the photosphere by inferring the motion of the surface field lines from photospheric magnetogram data, and
ii) inferring the rotation of the magnetic field vector from *in situ* data obtained by spacecraft located near the Earth.

If we find complete agreement of the helicity signs between CMEs and ICMEs, this result would support the hypothesis that all ICMEs are flux ropes. We investigate 34 CME–ICME events. To obtain the helicity sign of the ICMEs, we employ the fitting technique developed by Marubashi (2000) using the constant-$\alpha$ force-free field solution, assuming the

flux rope to be a cylinder with self-similar expansion. We do not consider the amount of helicity in this study since it could be different depending on the fitting model employed (Hu and Dasgupta, 2005; Marubashi and Lepping, 2007). On the contrary, we note that the sign of helicity determined by different fitting models is consistent between models. For this reason, we compare the helicity sign in ICMEs and to that in their source regions.

The rest of the paper is organized as follows. In Section 2, we describe briefly the methods used to determine the helicity injection rate. The helicity sign comparison between photospheric injection and ICME is given in Section 3, with detailed inspection of the four sign-inconsistent events. Section 4 summarizes the findings of this study.

## 2. Data and Analysis

The CDAW events (http://cdaw.gsfc.nasa.gov/meetings/2010_fluxrope/) have been selected from the list of shock-driving ICMEs in Gopalswamy *et al.* (2010), which originate from the vicinity of central meridian of the Sun (E15° $\leq$ source longitude $\leq$ W15°). To get a reliable helicity injection avoiding the projection effect on the line-of-sight magnetic field, we need continuous SOHO/MDI magnetogram (Scherrer *et al.*, 1995) data of the solar source region covering more than 24 hr without data gaps during the transit of the source region across the solar disk center. With this criterion, we select 28 events from the 54 CDAW events and also select six events from the list in Sung *et al.* (2009). Details of the identification of solar source regions associated with the 28 ICMEs are described in Gopalswamy *et al.* (2010), and those of the additional six CME–MC pairs can be found in Manoharan *et al.* (2004) and Qiu *et al.* (2007).

Detailed information on the 34 CME–ICME pairs are given in Table 1. The first column of Table 1 denotes the event number. Year, appearance time, speed, and angular width of the CMEs determined from SOHO/LASCO observations are listed from the second to fifth columns. The sixth to ninth columns contain information on the associated flare onset time and class, active region number, and solar source location, respectively. The last three columns give the start and end times of ICMEs, and their classification as listed in the CDAW ICME data table. Note that there are 24 MCs and 10 EJs in the dataset. We determined the geometry of the ICMEs and derived the helicity sign by assuming that the ICMEs have flux rope structure.

### 2.1. Photospheric Helicity Injection

The helicity sign in the solar source ARs of the selected events is obtained from the helicity flux density (*i.e.*, helicity injection per unit area per unit time) at the photospheric level of the ARs. To calculate the helicity flux density, we use the formula proposed by Pariat, Démoulin, and Berger (2005) and the numerical calculation method developed by Chae (2007).

Following the method of Chae (2007), we estimate the normal component of magnetic field ($B_n$) from the line-of-sight component of magnetic field ($B_l$), assuming that the magnetic field at the photosphere is normal to the solar surface and the transverse component of the magnetic field is negligible compared to $B_l$. This assumption is valid only in the case of active regions located near the solar disk center.

The time-dependent measurement of $B_l$ is obtained from a set of the full-disk 96 minutes SOHO/MDI (Scherrer *et al.*, 1995) magnetogram data. To reduce the geometrical projection effects in the calculation of $B_n$, we restrict to solar source regions located within 60 % of

**Table 1** Characteristics of flare, CME, and ICME.

| No[a] | Year | CME appearance Time | CME speed ($km\,s^{-1}$) | CME AW (deg) | Flare onset (UT) | Flare class | AR | Solar source Loc | ICME start[c] (UT) | ICME end (UT) | MC/EJ |
|---|---|---|---|---|---|---|---|---|---|---|---|
| C2 | 1997 | 05/12 05:30 | 464 | 360 | 04:42 | C1.3 | 8038 | N21W08 | 05/15 09:06 | 05/16 01:06 | MC |
| S11 | 1998 | 02/28 12:48 | 176 | 169 | – | – | 8171 | S24W01[b] | 03/04 19:00 | 03/06 05:00 | MC |
| C5 | 1998 | 05/02 14:06 | 938 | 360 | 13:31 | X1.1 | 8210 | S15W15 | 05/04 10:00 | 05/05 01:15 | EJ |
| S13 | 1998 | 06/21 05:35 | 192 | 163 | – | – | 8243 | N17W25[b] | 06/24 13:00 | 06/25 22:00 | MC |
| C16 | 2000 | 02/17 21:30 | 728 | 360 | 20:17 | M1.3 | 8872 | S29E07 | 02/21 09:48 | 02/22 13:18 | MC |
| C17 | 2000 | 07/07 10:26 | 453 | 360 | 08:42 | C5.6 | 9070 | N17E10 | 07/11 01:30 | 07/11 11:22 | EJ |
| C18 | 2000 | 07/08 23:50 | 483 | 161 | 22:58 | C4.0 | 9070 | N18W12 | 07/11 22:48 | 07/13 02:25 | EJ |
| C19 | 2000 | 07/14 10:54 | 1674 | 360 | 10:03 | X5.7 | 9077 | N22W07 | 07/15 21:06 | 07/16 09:54 | MC |
| C21 | 2000 | 07/25 03:30 | 528 | 360 | 02:43 | M8.0 | 9097 | N06W08 | 07/28 21:06 | 07/29 10:06 | MC |
| C23 | 2000 | 08/09 16:30 | 702 | 360 | 15:19 | – | 9114 | N20E12 | 08/12 06:06 | 08/13 05:06 | MC |
| C24 | 2000 | 09/16 05:18 | 1215 | 360 | 04:06 | M5.9 | 9165 | N14W07 | 09/18 01:54 | 09/18 15:06 | MC |
| C26 | 2000 | 10/09 23:50 | 789 | 360 | 23:19 | C6.7 | 9182 | N01W14 | 10/13 18:24 | 10/14 16:54 | MC |
| S26 | 2001 | 03/16 03:50 | 271 | 281 | – | – | 9384 | N11W09[b] | 03/19 19:00 | 03/22 06:00 | MC |
| C32 | 2001 | 04/10 05:30 | 2411 | 360 | 05:06 | X2.3 | 9415 | S23W09 | 04/12 07:54 | 04/12 17:54 | MC |
| C27 | 2001 | 04/19 12:30 | 392 | 129 | – | – | 9434 | N20W20[b] | 04/22 00:00 | 04/23 00:00 | MC |
| C33 | 2001 | 04/26 12:30 | 1006 | 360 | 11:26 | M1.5 | 9433 | N20W05 | 04/29 01:54 | 04/29 12:54 | MC |
| S30 | 2002 | 03/20 17:54 | 603 | 360 | – | – | 9871 | S17W20[b] | 03/24 03:00 | 03/25 22:00 | MC |
| C37 | 2002 | 04/15 03:50 | 720 | 360 | 03:05 | M1.2 | 9906 | S15W01 | 04/18 04:18 | 04/19 02:18 | MC |
| C39 | 2002 | 05/16 00:50 | 600 | 360 | 00:11 | C4.5 | 9948 | S23E15 | 05/19 03:54 | 05/19 23:24 | MC |
| C42 | 2002 | 07/15 21:30 | 1300 | 180 | 21:03 | M1.8 | 10030 | N19W01 | 07/18 12:00 | 07/19 08:10 | EJ |

**Table 1** (*Continued*)

| No[a] | Year | CME appearance Time | CME speed ($km\,s^{-1}$) | CME AW (deg) | Flare onset (UT) | Flare class | AR | Solar source Loc | ICME start[c] (UT) | ICME end (UT) | MC/EJ |
|---|---|---|---|---|---|---|---|---|---|---|---|
| C44 | 2003 | 08/14 20:06 | 378 | 360 | 17:12 | – | 10431 | S10E02 | 08/18 11:36 | 08/19 04:24 | MC |
| C45 | 2003 | 10/28 11:30 | 2459 | 360 | 11:00 | X17.2 | 10486 | S10E08 | 10/29 08:00 | 10/30 04:00 | MC |
| C46 | 2003 | 10/29 20:54 | 2029 | 360 | 20:37 | X10.0 | 10486 | S15W02 | 10/31 02:00 | 10/31 13:00 | MC |
| S32 | 2003 | 11/18 08:50 | 1660 | 360 | 08:30 | M3.9 | 10501 | N03E08[b] | 11/20 11:00 | 11/21 01:00 | MC |
| C48 | 2004 | 07/22 08:30 | 899 | 132 | 07:41 | C5.3 | 10652 | N04E10 | 07/24 12:48 | 07/25 13:18 | MC |
| C49 | 2004 | 11/06 02:06 | 1111 | 214 | 01:40 | M3.6 | 10696 | N09E05 | 11/09 20:54 | 11/10 03:24 | MC |
| C50 | 2004 | 12/08 20:26 | 611 | 360 | 19:34 | C2.5 | 10709 | N05W03 | 12/12 12:00 | 12/13 06:00 | EJ |
| C51 | 2005 | 01/15 06:30 | 2049 | 360 | 05:54 | M8.6 | 10720 | N16E04 | 01/16 14:00 | 01/17 06:30 | EJ |
| C52 | 2005 | 02/13 11:06 | 584 | 151 | 10:28 | C2.7 | 10733 | S11E09 | 02/18 15:00 | 02/19 08:15 | EJ |
| C53 | 2005 | 05/13 17:12 | 1689 | 360 | 16:13 | M8.0 | 10759 | N12E11 | 05/15 05:42 | 05/15 22:12 | MC |
| C54 | 2005 | 05/17 03:26 | 449 | 273 | 02:31 | M1.8 | 10763 | S15W00 | 05/20 07:18 | 05/21 05:18 | MC |
| C55 | 2005 | 05/26 21:26 | 420 | 199 | 20:57 | C8.6 | 10767 | S08E11 | 05/29 10:15 | 05/29 14:45 | EJ |
| C56 | 2005 | 07/07 17:06 | 683 | 360 | 16:07 | M4.9 | 10786 | N09E03 | 07/10 10:30 | 07/12 04:00 | EJ |
| C57 | 2005 | 08/31 11:30 | 825 | 360 | 10:26 | C2.0 | 10803 | N13W13 | 09/02 19:03 | 09/03 06:00 | EJ |

[a]'C' denotes that the CME–ICME pair is selected from the CDAW ICME list. 'S' denotes that CME–ICME pair is selected from Sung *et al.* (2009).

[b]Source ARs given by Manoharan *et al.* (2004) and Qiu *et al.* (2007) are used.

[c]ICME start time is the time when the leading boundary of the ICME is observed *in situ*, determined from fitting of the cylinder model.

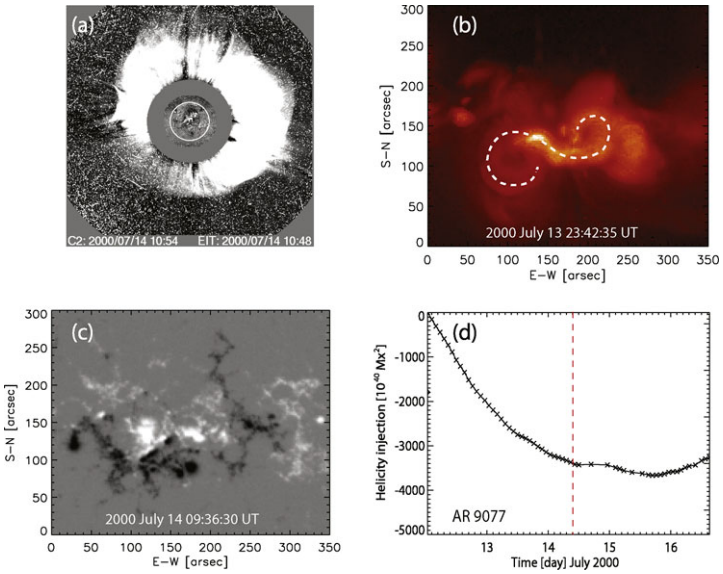


**Figure 1** (a) A SOHO/LASCO running difference image of the 14 July 2000 CME, (b) inverse-S shape sigmoid in a *Yohkoh* soft X-ray image of AR 9077, (c) MDI magnetogram of the AR, (d) estimated helicity injection in the AR from 12 to 16 July in 2000. The dashed vertical line in panel (d) denotes the start time of the flare associated with the CME.

the solar radius ($R_\odot$) from the apparent disk center. The velocity of the apparent horizontal motion of field line footpoints is determined by applying the differential affine velocity estimator (DAVE) method (Schuck, 2006). It is noted by Chae and Sakurai (2008) that the performance of DAVE is degraded in the presence of superpixel motions, even though DAVE outperforms the local correlation tracking (LCT) method. This comes from the linear assumption in DAVE that the speed of the motion is low enough.

We integrate the helicity flux density over the area of the region of interest (ROI) and also with respect to time to obtain the helicity injection ($\Delta H$) in the ROI. Finally, the sign of helicity in the ROI of the ARs is determined by the sign of $\Delta H$ at the occurrence time of the CMEs. Note that the start time of the helicity measurements is determined as soon as the ROI appears or rotates to a position within 0.6 $R_\odot$ from the disk center. Details of the procedure for the calculation of the photospheric helicity injection can be found in Chae (2007).

Figure 1 shows (a) the 14 July 2000 CME observed by SOHO/LASCO (Brueckner *et al.*, 1995) C2, (b) a *Yohkoh*/SXT (Tsuneta *et al.*, 1991) soft X-ray image of the source AR of the CME, NOAA 9077, (c) a SOHO/MDI magnetogram of the AR, and (d) helicity injection ($\Delta H$) in the entire AR. The vertical dashed line in Figure 1(d) indicates the start time of the flare associated with the CME. As shown in Figure 1(d), helicity with a negative (left-handed) sign was continuously injected through the entire photospheric surface of the AR from 12 July up to the onset of the flare. We therefore conjecture that the CME produced in the AR has helicity with a negative sign.

In fact, the CME was observed as an ICME near the Earth on 15 July 2000, and the cylinder fitting models of the ICME indicate that it had a flux rope structure and its helicity sign was negative. In Section 2.2, we describe in detail the ICME fitting model that was used in this study.

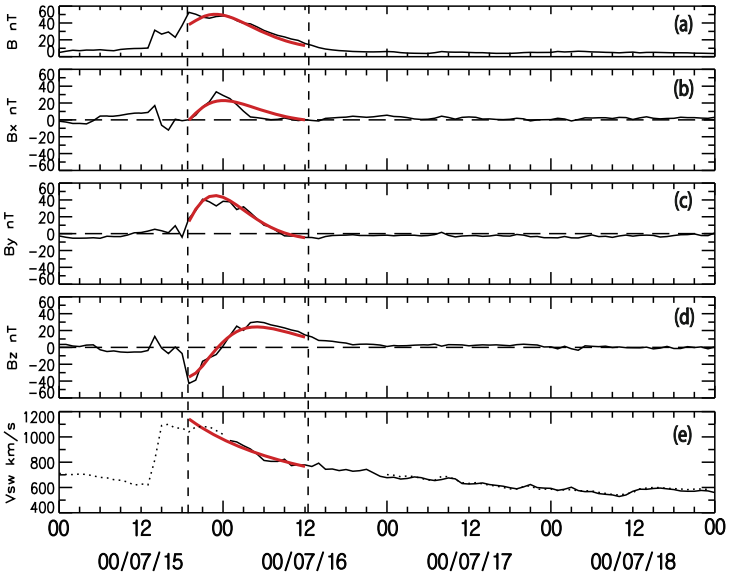


**Figure 2** *In situ* interplanetary space data from the ACE spacecraft showing (a) total magnetic field strength, (b) to (d) magnetic field vector in GSE coordinates and (e) solar wind speed. The result of the fitting of the cylinder model is shown by the thick, solid, red lines. The ICME boundaries are located at 19:00 UT on 15 July and 12:00 UT on 16 July 2000, indicated by the two vertical dashed lines.

## 2.2. Magnetic Cloud Helicity Sign

We perform the cylinder model fitting for 34 ICMEs with either the 15, 20, 30, or 60 mins averaged magnetic field data from the *Magnetic Field Experiment* (MAG: Smith *et al.*, 1998) on the *Advanced Composition Explorer* (ACE) spacecraft, depending on the duration of the ICME. We select the ICME time interval in which the magnetic field vectors change direction smoothly in the $Y - Z$ GSE plane. We then adjust the time span of the ICMEs and the optimum fitting parameters, such as the bulk velocity, intensity of the magnetic field at the cylinder axis, radius of the cylinder, geometry and expansion rate of the cylinder, and the helicity sign of the ICME, which are selected when the least-squares fitting procedure returns a result that is most consistent with the magnetic field observations. In general the helicity sign of an ICME can be judged from the direction of magnetic field rotation with respect to the Earth–Sun line: the helicity is positive (negative) when the rotation has right-handed chirality (left-handed chirality). However, there are some cases where the magnetic field rotation is not very clear. Therefore, we tried the fitting for positive and negative helicity sign when necessary, and selected the helicity sign which yielded a better fit. It is noted that adjustment of the start and end times of the fitting is sometimes necessary for the best fit. We have found that the adjustment is usually less than a few hours and only a little different from Lepping's fit, which can be found in the CDAW list. The difference does not give significantly different results. A detailed description of the cylinder model, the parameters, and fitting procedure are explained by Marubashi and Lepping (2007), and references therein. The start and end times of ICMEs for the best fit using the cylinder model are listed in Table 2.

Figure 2 presents the results of the cylinder fitting for the ICME detected on 15 July 2000 at 21:06 UT associated with the 14 July 2000 CME (Figure 1(a)). From top to bottom, the

**Table 2** Estimated helicity injections in the active region and inferred quantities of the magnetic flux in the ICMEs.

| No[a] | Active region | | | | | ICME | | | | |
|---|---|---|---|---|---|---|---|---|---|---|
| | Start date[c] | Start time[c] | $H_{acc}$ ($10^{40}$ $Mx^2$) | AR sig. | Arcade clear? | Start time | End time | Cylinder $\theta$[d] | Cylinder $\phi$[e] | Helicity sign |
| C2 | 970509 | 14:28 | −100 | IS | Yes | 05/15 09:50 | 05/16 02:20 | −5 | 95 | LH |
| S11 | 980226 | 11:12 | −15 | IS(?) | No | 03/04 19:00 | 03/06 5:00 | 28 | 77 | LH |
| C5 | 980428 | 19:10 | 2300 | S | Yes | 05/05 13:00 | 05/06 02:00 | 7 | 309 | RH |
| S13 | 980616 | 17:36 | −450 | IS | No | 06/24 13:00 | 06/25 22:00 | 34 | 131 | LH |
| C16 | 000216 | 06:23 | 600 | S | Yes | 02/21 13:00 | 02/22 12:00 | 80 | 322 | RH |
| C17 | 000706 | 00:00 | −2700 | IS | Yes | 07/11 03:30 | 07/11 13:30 | −7 | 343 | LH |
| C18 | 000706 | 00:00 | −4800 | IS | Yes | 07/11 22:30 | 07/13 04:30 | 47 | 61 | LH |
| C19 | 000712 | 00:00 | −4500 | IS | Yes | 07/15 19:30 | 07/16 12:30 | 19 | 63 | LH |
| C21[b] | 000722 | 07:59 | 950 | IS(?) | No | 07/28 14:00 | 07/29 00:30 | 58 | 376 | LH |
| C23 | 000806 | 11:15 | −3100 | IS | Yes | 08/12 05:00 | 08/13 06:00 | 15 | 115 | LH |
| C24 | 000913 | 09:33 | −2300 | IS | Yes | 09/17 23:20 | 09/18 14:20 | 41 | 226 | LH |
| C26[b] | 001006 | 12:47 | −200 | S(?) | Yes | 10/13 16:30 | 10/14 14:00 | −24 | 42 | RH |
| S26 | 010313 | 08:00 | −50 | ? | No | 03/19 20:00 | 03/22 6:00 | −65 | 128 | LH |
| C32 | 010407 | 04:48 | 210 | S(?) | Yes | 04/12 06:00 | 04/13 03:00 | 1 | 353 | RH |
| S27 | 010418 | 08:00 | −6 | S | Yes | 04/22 00:00 | 04/23 03:00 | −50 | 308 | LH |
| C33 | 010423 | 11:12 | −6200 | IS | Yes | 04/29 00:30 | 04/29 14:00 | 0 | 115 | LH |
| S30 | 020317 | 03:15 | 700 | IS | Yes | 03/24 20:30 | 03/25 20:30 | 23 | 203 | RH |
| C37 | 020412 | 09:36 | 6500 | S | Yes | 04/18 01:00 | 04/19 10:00 | −17 | 323 | RH |
| C39 | 020514 | 19:15 | 400 | IS(?) | Yes | 05/19 02:45 | 05/19 22:45 | 9 | 234 | RH |
| C42 | 020713 | 12:51 | −1100 | ? | No | 07/18 12:00 | 07/18 21:40 | 39 | 29 | LH |

**Table 2** (*Continued*)

| No[a] | Active region | | | | | ICME | | | | |
|---|---|---|---|---|---|---|---|---|---|---|
| | Start date[c] | Start time[c] | $H_{acc}$ ($10^{40}$ $Mx^2$) | AR sig. | Arcade clear? | Start time | End time | Cylinder $\theta$[d] | Cylinder $\phi$[e] | Helicity sign |
| C44 | 030812 | 22:23 | 2400 | S | Yes | 08/18 10:30 | 08/19 15:30 | −15 | 312 | RH |
| C45 | 031027 | 07:59 | −6700 | IS | Yes | 10/29 11:00 | 10/30 02:00 | −54 | 229 | LH |
| C46 | 031027 | 07:59 | −10600 | IS(?) | Yes | 10/31 02:30 | 11/01 00:30 | 49 | 235 | LH |
| S32[b] | 031117 | 04:51 | −450 | IS | Yes | 11/20 11:00 | 11/21 00:30 | −66 | 137 | RH |
| C48 | 040720 | 23:59 | 4000 | S | No | 07/24 17:30 | 07/25 06:30 | −13 | 41 | RH |
| C49 | 041103 | 23:59 | −4500 | S | Yes | 11/10 03:00 | 11/11 01:00 | −33 | 160 | LH |
| C50 | 041206 | 08:00 | −290 | IS | Yes | 12/13 07:00 | 12/13 21:00 | −25 | 162 | LH |
| C51 | 050113 | 12:47 | −2100 | IS | No | 01/16 16:20 | 01/17 01:20 | −2 | 237 | LH |
| C52 | 050211 | 09:39 | 610 | S | No | 02/18 17:30 | 02/19 04:00 | 22 | 277 | RH |
| C53 | 050512 | 01:35 | −240 | IS | Yes | 05/15 06:00 | 05/16 04:00 | 49 | 159 | LH |
| C54[b] | 050514 | 11:15 | 10 | S(?) | No | 05/20 15:10 | 05/21 06:10 | 20 | 231 | LH |
| C55 | 050525 | 14:23 | −400 | S(?) | No | 05/29 10:30 | 05/29 14:45 | 11 | 184 | LH |
| C56 | 050705 | 01:35 | −700 | IS | No | 07/10 17:00 | 07/11 00:30 | −36 | 23 | LH |
| C57 | 050828 | 06:23 | 210 | S | Yes | 09/02 19:20 | 09/03 04:00 | 1 | 173 | RH |

[a] 'C' denotes that the CME–ICME pair is selected from the CDAW ICME list. 'S' denotes that CME–ICME pair is selected from Sung *et al.* (2009).

[b] Exceptional events whose helicity signs of MC and AR are not consistent.

[c] Start date and time of helicity measurement of the source region.

[d] $\theta$ is the latitude angle of the cylinder axis magnetic field.

[e] $\phi$ is the longitude angle of the cylinder axis magnetic field.

panels show the total magnetic field intensity, $X$-, $Y$-, and $Z$-components of the magnetic field in the GSE coordinates, and solar wind speed, respectively. The vertical dashed lines denote the start and end times of the ICME that give the best fit to the observations. The thick red solid lines are the results of the fitting with the cylinder model, which show excellent agreement with the observations. The determined helicity sign of the ICME is negative, and the latitude ($\theta$) and longitude ($\phi$) of the axis of the ICME are 19° and 63°, respectively. The fitting results for the rest of the events are shown in Table 2.

## 3. Results

### 3.1. Helicity Sign Comparison

Table 2 summarizes the results on helicity accumulation in the source ARs and the fitting results for the 34 ICMEs. The first four columns give the event number, the start date and time of helicity accumulation measurements, and the accumulated helicity within the AR between the start time of the accumulation and the onset time of the flare. The fifth and sixth columns present the deduced sigmoid shape of the AR using *Yohkoh*/SXT images and the clearness of the post-eruption arcade (PEA) structure after the eruption to identify whether it has S- or Inverse S-shape. Those with a shape and a question mark *e.g.* 'IS(?)' events are where we think the sigmoid shape is an inverse S, but there is some uncertainty, while those with just a question mark do not show any evidence of the presence of a sigmoid.

According to the coronal flux rope (CFR) model (Titov and Démoulin, 1999), a toroidal flux rope is embedded in an active region with a dipolar flux system. The projected magnetic separatrix surface has an S-shape when the flux rope is right-handed (positive helicity), while it has an inverse S-shape when it is left-handed (negative helicity). Employing the CFR model, we find that about 61 % (21/34) of the ICMEs have the same helicity sign as that deduced from the X-ray sigmoid shape, while for 11 % (4/34) of the ICMEs the deduced signs disagree. However, we find that there are many ambiguities (9/34, 26 %) in the determination of the sigmoid shape through inspection directly from soft X-ray images. We thus conclude that the sigmoid analysis needs careful treatment and high resolution loop observations.

The next five columns present the start and end times of ICMEs for the fitting, the $\theta$ and $\phi$ of the cylinder axis in GSE coordinates, and the helicity sign of ICME determined from the cylinder model. The orientation of magnetic cloud axes is described in terms of $\theta$ and $\phi$, where $\theta$ is the angle between the magnetic cloud axis and the ecliptic plane and $\phi$ is the angle between $X$gse and the projection of the magnetic cloud axis on the ecliptic plane, measured positive when anti-clockwise (right-handed chirality). The direction of the ICME axis projected onto the $Y-Z$ plane can be estimated using the equation given by Marubashi *et al.* (2012).

For statistical evaluation of the sign consistency, we have compared the accumulated helicity sign of the solar source region with the relative helicity sign inferred from the structure of the ensuing ICME as shown in Table 3. We find that 30 events (88 %) have the same helicity sign while four events (C21, C26, S32, and C54 in Table 2) have different signs.

### 3.2. Sign-Inconsistent Events

Based on the helicity conservation principle, we have investigated the four exceptional events in detail with the speculation that their signs may be inconsistent for one of the following reasons:

**Table 3** Helicity sign comparison between ICME and solar source active region.

| ICME | Solar source AR | | Total |
|---|---|---|---|
| | Positive | Negative | |
| Positive | 10 | 3 | 13 |
| Negative | 1 | 20 | 21 |
| Total | 11 | 23 | 34 |

i) wrong identification of the solar source region,
ii) the wrong selection of CME–ICME pair, or
iii) localized helicity injection with different helicity sign than the sign of helicity in the entire source active region.

### *3.2.1. 28 July 2000 ICME (Event C21 in Table 2)*

According to the *Solar Geophysical Data* (SGD; ftp://ftp.ngdc.noaa.gov/STP/space-weather/solar-data/solar-features/solar-flares/x-rays/goes/), an M8.0 flare occurred at 02:43 UT on 25 July 2000 in AR9097 near the disk center (N06W08). After the flare, a halo CME appeared in the LASCO C2 field of view at 03:30 UT as seen in Figure 3(b). The CME arrived at the Earth with an IP shock on July 28. The IP shock was detected by the ACE satellite at 05:43 UT on the same day, as denoted by a vertical dashed line in Figure 3(c). We set the start and end times of the ICME to July 28 14:00 UT and July 29 00:30 UT for the boundaries of the flux rope structure, respectively, and determine its helicity sign by using the cylinder model. The deduced helicity sign of the ICME is negative. The estimated axis direction of the ICME projected on the $Y - Z$ GSE plane using the cylinder model for the above boundaries of the ICME is about 80°.

We examine AR9097, which is reported in the CDAW ICME list as the solar source region of the CME. The helicity injections through the entire active region and the polarity inversion line (PIL) region, marked with a white box in Figure 3(a), have positive signs which are not the same as that of the ICME. It is noted that there are several filaments which might be related to the CME as shown in BBSO Hα image (Figure 3(d)). We have considered the filaments as possible candidates for the CME, and we have investigated the Hα images taken before and after the flare. In the case of the filament North of the AR, it disappeared at 01:44 UT, before the flare. There were two filaments in regions F1 and F2 which disappeared after the flare. Due to a data gap in the Hα observations, the exact times of these filament eruptions cannot be identified. We inspect the helicity injection in these regions. As shown in Figure 3(i), the accumulated helicity in the F1 region has a negative sign but there is no significant helicity injection in the region F2, so the filament from the region F1 seems to be the most likely candidate for the source region of the CME.

During the flare time, there was another eruption from AR 9096 located to the South of AR 9097 as marked by the yellow box in Figure 3(a). The filament eruption can be clearly seen in Hα data from Yunnan observatory and in the movie from the SOHO/LASCO CME catalog (http://cdaw.gsfc.nasa.gov/CME_list; Yashiro *et al.*, 2004; Gopalswamy *et al.*, 2009). The eruption started at about 02:46 UT and we can see a clear Post-Eruption Arcade (PEA) structure in the *Yohkoh* SXT image shown in Figure 4(c). For the filament region, R3, we estimate the helicity injection and find a negative helicity sign, the same as that of the ICME.

We find two candidate solar source regions (F1 and F3) for the CME, which have negative helicity accumulation. If we assume that the flux rope of a CME that erupts from an AR

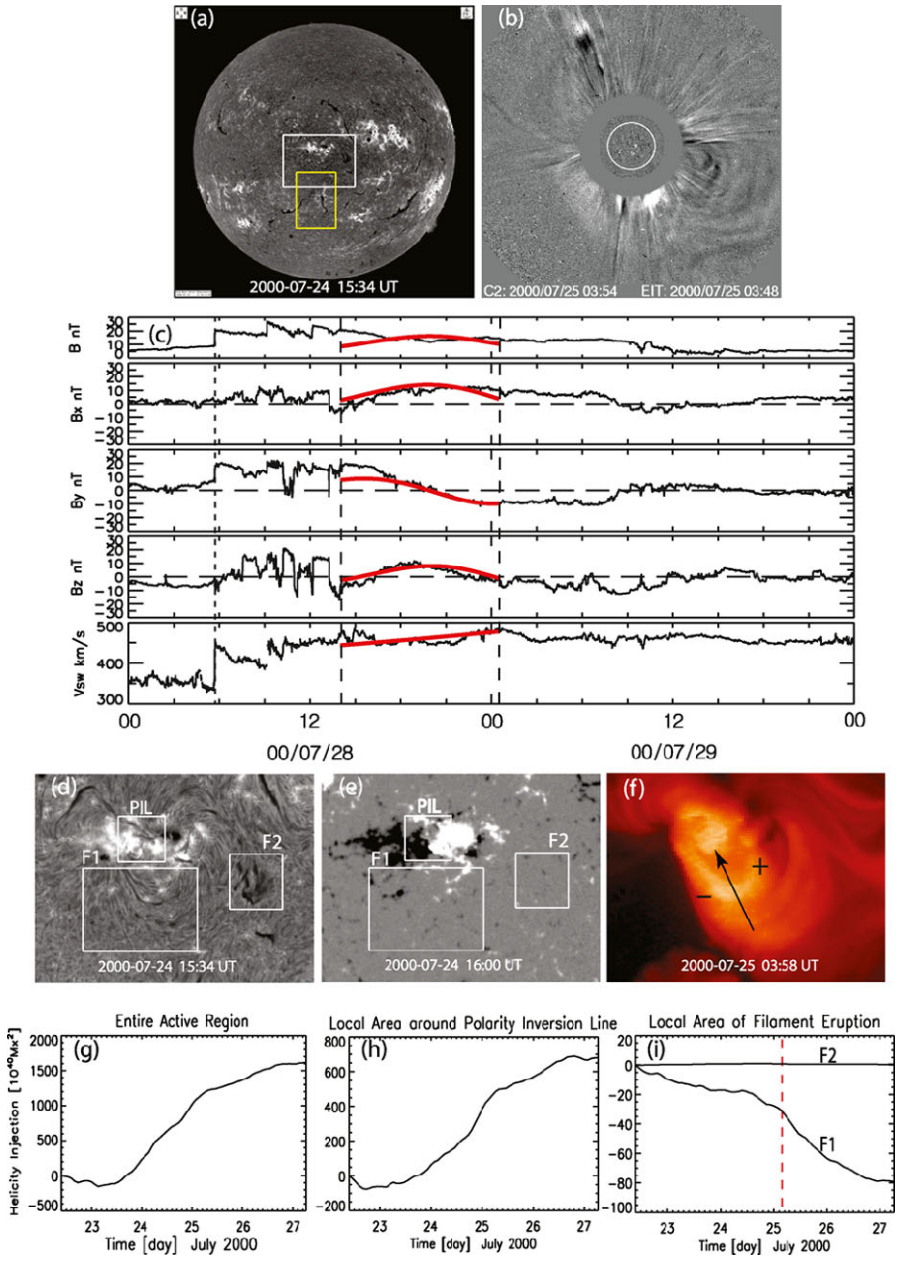


**Figure 3** The 25 July 2000 CME, the associated 28 July 2000 ICME and the candidate solar source regions. (a) Full disk BBSO H$\alpha$ image. The white and yellow boxes denote the locations of AR 9097 and AR 9096, respectively. (b) Shows LASCO C2 observations of the CME that produced the ICME observed *in situ* near Earth, shown in (c). Solid, red lines denote a fitting result of the cylinder model. The vertical dotted and dashed lines represent the time of arrival of the interplanetary shock and the boundaries of the ICMEs, respectively. Submaps focusing on AR 9097 prior to the CME eruption are shown in (d) H$\alpha$ and (e) a magnetogram from SOHO/MDI. (f) Shows *Yohkoh*/SXT observations of the same region post-eruption. Estimates of helicity injection in the regions of interest are shown for (g) the entire active region, (h) the polarity inversion line (PIL) and (i) the regions labeled 'F1' and 'F2'. The red, vertical line indicates when the flare occurred.

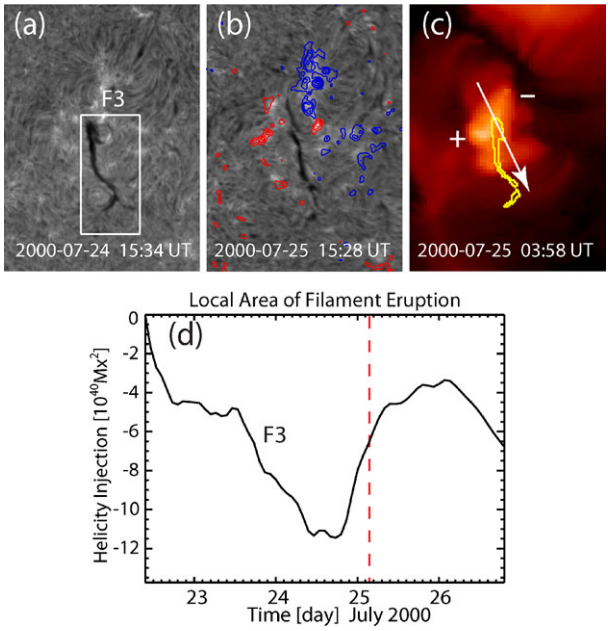


**Figure 4** BBSO Hα submap images of AR 9096 (a) before and (b) after the CME. (c) Shows a *Yohkoh* SXT submap image after the CME and (d) shows the helicity injection in the filament region of AR 9096. The filament region (F3) is denoted by a white box in the local Hα image. The red and blue contours on the BBSO Hα image after the CME denote positive and negative magnetic fields observed by SOHO/MDI, respectively. The red vertical line indicates when the flare occurred.

maintains its axis orientation (Yurchyshyn *et al.*, 2001) as it propagates from the Sun to the Earth and the flux rope is assumed to be observed at (or near) the apex of the ICME loop, the orientation of the ICME axis projected onto the $Y-Z$ plane may be aligned with the direction of the flux rope structure near the Sun, which can be estimated from the orientation of the PEA associated with the eruption. Based on this assumption, we adopt the alignment of the flux rope axes as a second constraint to select the solar source region of ICME, and measure the orientation angles of the axes of PEAs. Figure 3(f) and Figure 4(c) show the PEAs in the regions F1 and F3. By considering the helicity sign and magnetic polarities from MDI data, we can determine the axial direction of each of the PEAs by measuring the angle from the East on the Sun in a clockwise (left-handed chirality) direction. For the F1 region in AR 9097, the estimated PEA axis angle is about 65° as marked by an arrow in Figure 3(f) and that of the PEA in AR 9096 is about 270°. Since the axis angle of the PEA in AR 9097 is roughly similar to that (80°) of the ICME estimated using the cylinder model and their helicity signs are same, we conclude that the region F1 in AR9097 is the most probable source region of the 28 July 2000 ICME. Prior to this study, an incorrect association had been made between the ICME and its source region, which originally led to the incorrect conclusion that the helicity sign was not conserved between the solar source region of the CME and the associated ICME.

### *3.2.2. 13 October 2000 ICME (Event C26 in Table 2)*

According to the CDAW ICME list, the ICME of 13 October 18:24 UT to 14 October 16:54 UT was associated with the halo CME that appeared at 00:26 UT on 10 October 2000 in the LASCO C2 FOV as shown in Figure 5(b). The linear speed of the CME in the plane of sky from SOHO/LASCO observations is 527 km $s^{-1}$. This CME is related to the C6.7 flare from AR 9182 (the box in Figure 5(a)) at 23:19 UT located near the disk center (N01W41). The cylinder fitting result for the ICME during the period between 13 October 16:30 UT

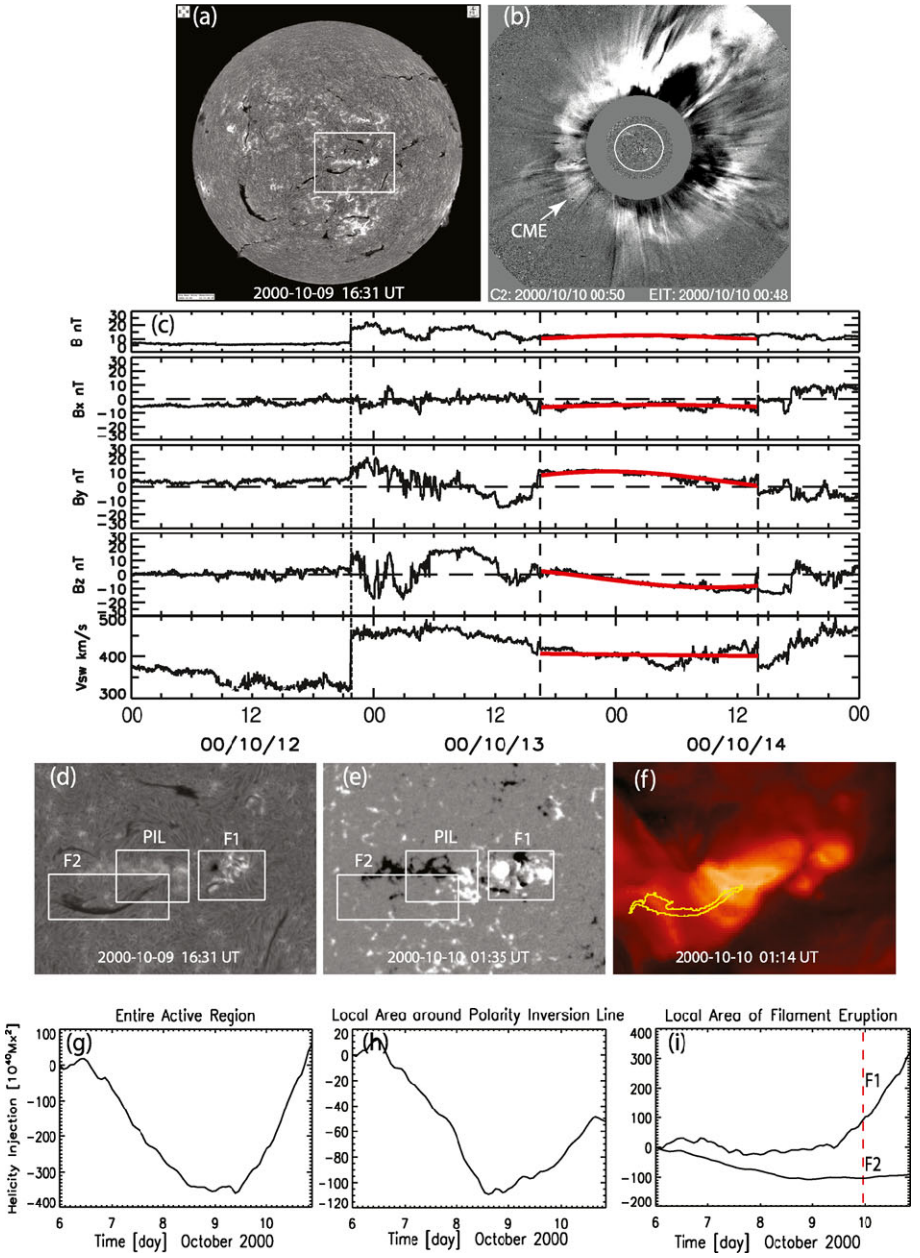


**Figure 5** The 9 October 2000 CME, the associated 13 – 14 October 2000 ICME and the candidate solar source regions. (a) Full disk BBSO H$\alpha$ image. The white box denotes the location of AR 9182. (b) Shows LASCO C2 observations of the halo CME that produced the ICME observed *in situ* near Earth, shown in (c). Solid red lines denote a fitting result of the cylinder model. The vertical dotted and dashed lines represent the arrival time of the interplanetary shock and the boundaries of the ICME. Submaps focusing on AR 9182 prior to the CME eruption are shown in (d) H$\alpha$ and (e) a magnetogram from SOHO/MDI. (f) Shows *Yohkoh*/SXT observations of the same region post-eruption. Estimates of helicity injection in the regions of interest are shown for (g) the entire active region, (h) the polarity inversion line (PIL), and (i) the regions labeled 'F1', and 'F2'. The red vertical line indicates when the flare occurred.

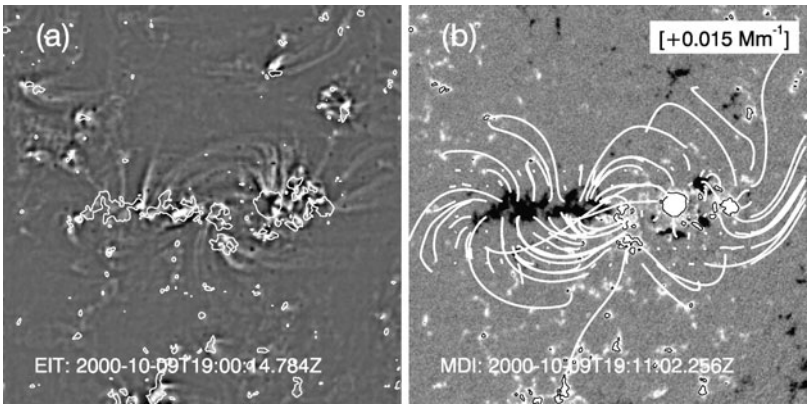


**Figure 6** Determination of the coronal magnetic helicity sign of AR9182, and its comparison with observed coronal loops. (a) SOHO/EIT image in gray scale with the magnetic field strength contours at $\pm 200$ G overlaid. (b) SOHO/MDI magnetogram in gray scale and the computed magnetic field lines projected onto the surface. The obtained best-fit $\alpha$ is $+0.015$ Mm$^{-1}$.

and 14 October 14:00 UT reveals that the ICME has a positive helicity sign, but the signs of injected helicity through the entire active region (AR 9182) and PIL are both negative (Figure 5(g) and (h)).

To identify the solar source region of the ICME, we have determined helicity signs for the local regions F1 and F2. As shown in Figure 5(i), it is found that the region F1 has positive, while the region F2 has negative injected helicity. There was a previous CME that was associated with the region F1. The CME appeared at 23:50 UT on 9 October in the LASCO C2 FOV with narrow angular width ($\sim 40°$). The linear speed of the CME was about 800 km s$^{-1}$. The CME from F1 could be a possible candidate for being the source region of the ICME. However, this does not look plausible, since it is difficult to explain how a narrow limb CME with small direction parameter can be detected near Earth as an ICME.

In addition to the helicity injection through the photosphere, we also have measured the sign of the helicity content in the corona using the linear force-free field (LFFF) model. The reliability of the LFFF model to measure the coronal magnetic helicity was demonstrated by previous studies (Démoulin *et al.*, 2002; Lim, Jeong, and Chae, 2007). The coronal magnetic field is extrapolated from the SOHO/MDI line-of-sight magnetogram using the Fourier transform method suggested by Alissandrakis (1981) by changing the value of the force-free $\alpha$. Then the computed coronal model is compared with the observed coronal loops to determine the best-fit $\alpha$. The best-fit $\alpha$ has the same sign as that of the coronal magnetic helicity.

Figure 6 shows the LFFF model with the obtained best-fit $\alpha$ (Figure 6(b)) compared with the observed coronal loops in the SOHO/EIT 171 Å image (Figure 6(a)). Since our concern is the sign of the coronal magnetic helicity, we have compared the overall topology of the coronal loops and the LFFF model. As a result, we obtain a positive value for the force-free $\alpha$ indicating that the AR9181 has positive magnetic helicity in the corona. The sign of the coronal magnetic helicity is the same as that of the helicity of the ICME. Projection effects have not been considered since the active region was near the disk center. Moreover, the barb structures of the filament shown in the H$\alpha$ image (F2 in Fig. 5(d)) indicate that the chirality of the filament is sinistral, in other words, it has positive helicity. Therefore, the sign of the computed coronal helicity is also consistent with that of the filament chirality

(Lim and Chae, 2009). The same filament was also visible on 5 October, and showed a sinistral structure. Therefore, it is likely that the sign of the coronal magnetic helicity was already positive at least from 5 October.

It has been reported that the local helicity sign can be opposite to that of the whole active region helicity (Hao and Zhang, 2011), and the injection of helicity with the opposite sign to that of the pre-existing helicity plays an important role in eruptive events such as flares and CMEs (Park *et al.*, 2012; Jing *et al.*, 2012). We speculate that overall the coronal field in AR9181 had pre-existing positive helicity and the local injection of negative helicity in the F1 region played a role through magnetic reconnection in the ejection of the pre-existing positive coronal helicity via the CME and ensuing ICME. We conclude that the helicity sign of the ICME is not consistent with the sign of injected helicity during the analyzed period, but it is consistent with that of the coronal helicity in the whole active region (AR9182).

### *3.2.3. 20 November 2003 ICME (Event S32 in Table 2)*

The ICME of 20 November 11:00 UT to 21 November 01:00 UT was caused by a halo CME (1660 km s$^{-1}$) that appeared at 08:50 UT on 18 November 2003 in the LASCO C2 FOV as seen in Figure 7(b). This CME is related to an M3.9 flare in AR 10501 (the box in Figure 7(a)) at 08:30 UT near the disk center (N03E08) and is known to be the most probable solar source of the ICME (Gopalswamy *et al.*, 2005). The cylinder fitting result for the ICME reveals that the ICME has a positive helicity sign, but the signs of injected helicity in the entire active region and along the PIL are negative as shown in Figure 7(g) and (h). The projected axis orientation angles of the ICMEs using the cylinder model is about 290°.

There was an erupting filament with a curved shape in region F1 as marked in Figure 7(d). The SOHO/EIT image after the eruption shows a PEA structure in the region as seen in Figure 7(f). The yellow contour in Figure 7(f) depicts the filament just before the flare. The EIT movie in the CDAW CME catalog also shows that the filament was gradually rising from 18 November 04:36 UT to 08:00 UT, and finally it erupted before 09:20 UT on 18 November. We speculate that this filament is the source of the CME because there is no other filament present at 09:20 UT in the Catania H$\alpha$ image. We estimate the injected helicity signs in the entire AR region and each local region such as the PIL region and the region F1 where the filament was located as shown in Figure 7(d). As a result, we find that the sign of injected helicity in the region F1 is positive, as shown in Figure 7(i), which is the same sign as that of the MC.

In fact, this event was reported by Chandra *et al.* (2010), who studied the solar source of the ICME, and by Gopalswamy *et al.* (2005), who studied the relationship between the CME and ICME. Chandra *et al.* (2010) examined the spatial distribution of magnetic helicity injection, and concluded that the positive helicity in the eastern part (F1a in Figure 8) of the filament was consistent with the ICME. However, Gopalswamy *et al.* (2005) reported that the eastern leg had erupted before the halo CME. They proposed that the entire filament erupted during the halo CME and the North-South segment (F1b in Figure 8) was the largest and may be responsible for the halo CME. In addition, they pointed out that the axis angle of the segment is consistent with the ICME axis orientation from the cylinder model.

Since the helicity sign in the corona where the helicity of both the filament and the CME originated from has not been fully explained in the work of Chandra *et al.* (2010), we have investigated this active region in detail. Similar to Section 3.2.2, we also apply the LFFF model to check the sign of the coronal helicity before the halo CME occurred. The overall coronal loops in the TRACE image agree with either the negative or near zero force-free $\alpha$, as in Chandra *et al.* (2010), except for the local dark loops indicated by an arrow in

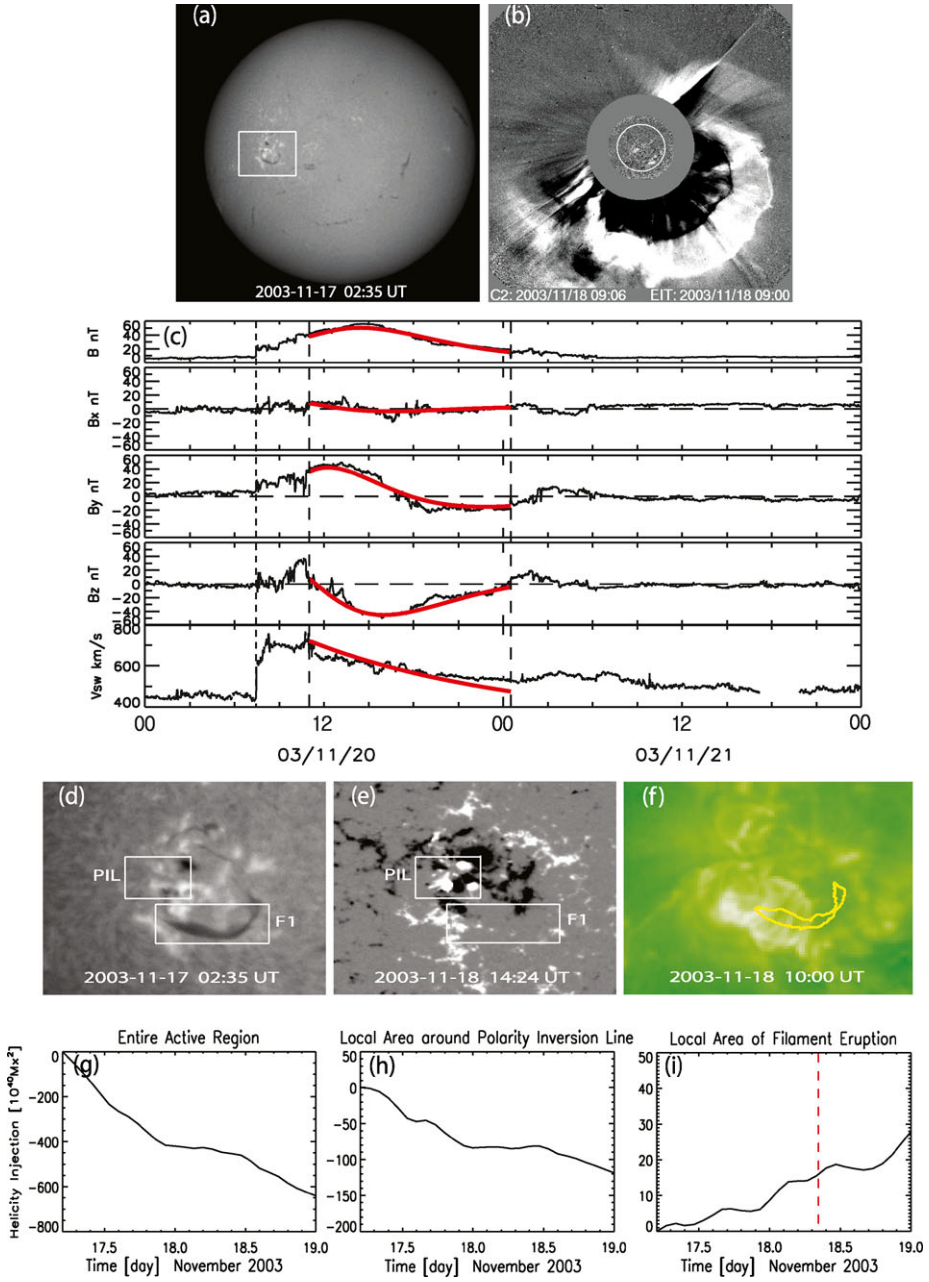


**Figure 7** The 18 November 2003 CMEs, the associated 20 November 2003 ICME, and the candidate solar source regions. The white box in the full disk Hα image (a) of Yunnan observatory denotes AR 10501. The CME in a LASCO C2 image (b) produced the ICME (c). Red thick lines in the panel (c) denote fitting results of the cylinder model and the vertical dotted and dashed lines represent the IP shock arrival time and the boundary of the ICME. Submap Hα images before (d) the CME are presented with a magnetic map of the same region from SOHO/MDI (e) and a SOHO/EIT image (f). Helicity injections are estimated for the entire AR 10501 (g), 'PIL' (h), and 'F1' regions (i), respectively. The red dashed vertical line indicates when the flare occurred.

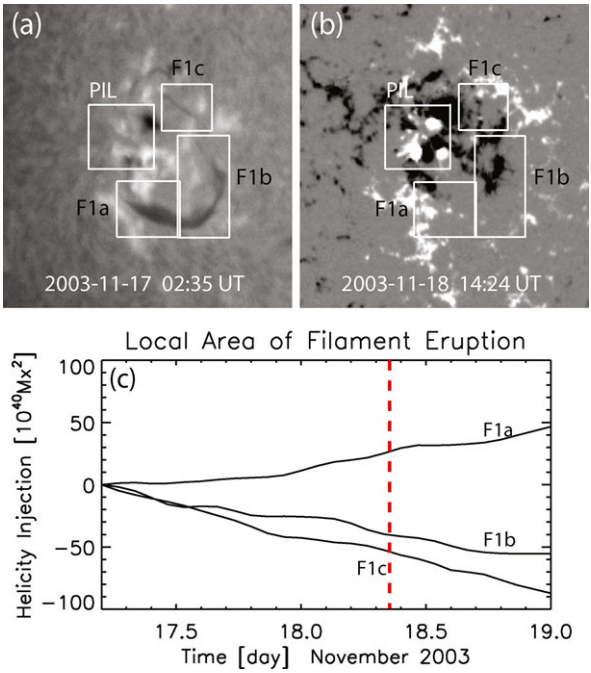


**Figure 8** Yunnan Hα submap image (a) and SOHO/MDI magnetogram (b) of AR 10501 before the CME. The helicity injections (c) are estimated for each segment of the filament. The red dashed vertical line indicates when the flare occurred.

Figure 9(a). Those dark loops seen in the TRACE image are the same filament shown in Figure 7(d) and Figure 8(a). We can reconstruct those dark loops in the lower region with positive force-free $\alpha$ (red field lines in Figure 9(b)), and the loops in the upper region with negative $\alpha$ (blue field lines on the right-hand side of the red lines). We have also overlaid the contour of the filament segment that erupted during the halo CME (black contour in Figure 9(b)). We find that the erupted filament has positive helicity in the corona. Our result supports the idea that the positive helicity sign of the ICME of interest originates from the locally positive coronal helicity, and this region becomes unstable and erupts facilitated by the opposite sign of helicity in this region to that of the surroundings (Park *et al.*, 2012; Jing *et al.*, 2012).

### *3.2.4. 20 May 2005 ICME (Event C54 in Table 2)*

The 20 May 2005 ICME had been reported by the CDAW to be caused by the 17 May 2005 CME that appeared at 03:26 UT in the LASCO C2 FOV. The CME is a partial halo CME and has a slow speed of 450 km $s^{-1}$. The deduced helicity sign of the ICME using the cylinder model is negative, and the fitting result shows good agreement with the observations, as shown in Figure 10(c).

In the solar source region of the CME (AR 10763), three flares occurred on 17 May. The first, second, and third flares started at 02:31 UT, 03:58 UT, and 05:47 UT in the western, middle, and eastern parts of the AR, respectively. There were two small filaments in the active region marked as F1 and F2 in Figure 10(d). The signs of injected helicity over the entire active region and the region of PIL are both positive as shown in Figure 10(g) and (h). The filament in the region F1 has negative helicity sign while the filament in the region F2 has positive sign (Figure 10(i)). Considering its time of appearance (03:26 UT), the CME is probably related to the first flare that occurred in the West of the AR at 02:31 UT on 17 May

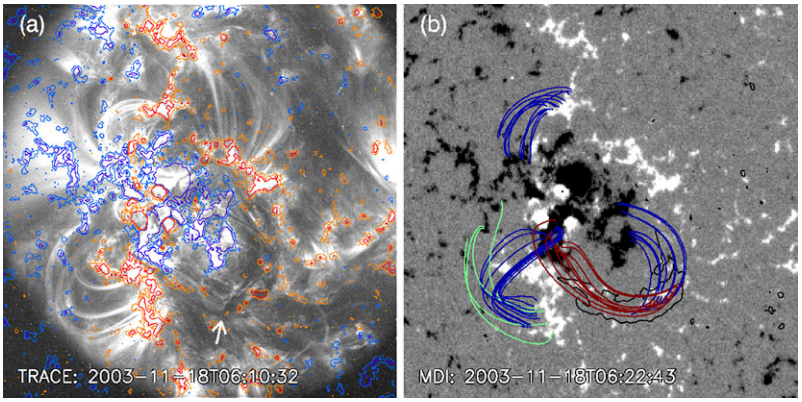


**Figure 9** Determination of the coronal magnetic helicity sign in AR10501, through magnetic extrapolation and its comparison with observed coronal loops. (a) TRACE 171 Å image and line-of-sight magnetic field contours from SOHO/MDI overlaid corresponding to (−200, −50, 50, 200 G) levels. (b) SOHO/MDI magnetogram and selected magnetic field lines computed from the linear force-free field extrapolation with different $\alpha$ values (green: 0, blue: negative, red: positive). Black contour represents the filament that disappeared after the CME (flare) obtained from Hα images taken by Kanzelhöhe Solar Observatory at 07:39:51 and 12:16:08 UT on 18 November 2003.

2005. The filament F1 seems to be a possible source of the ICME since it has the same helicity sign as that of the ICME, if the CME–ICME pair is correctly selected. However, we note that the filament in the F1 region can still be seen at 07:07 UT on 17 May in the Hα movies from the *Hida Domeless Solar Telescope* (http://fw.hida.kyoto-u.ac.jp), and no clear PEA structure can be seen in the EIT image, as shown in Figure 10(f). It is also noted that no PEA signature is found in SXI images. For these reasons, we conclude that the region F1 is not the source region of the ICME.

Meanwhile, another candidate solar source of the ICME was proposed by Zhang *et al.* (2007), who suggested that the 20 May 2005 MC may be due to a partial halo CME that appeared at 13:50 UT on 16 May 2005 in the LASCO C2 FOV as seen in Figure 11(b). The solar source region of the CME, AR 10759, located at N13W29 is denoted by a white box in Figure 11(a). We note that the CME was related to the eruptive filament located in region F1 of Figure 11(c). The eruption of the filament occurred at 12:12 UT on 16 May, and the eruption can be clearly seen in the H$\alpha$ movie by the *Solar Telescope of Argentina* (HASTA, http://www.oafa.fcefn.unsj-cuim.edu.ar). We inspect helicity injections over the entire region, PIL region, and F1 filament region of AR 10759, and find that they all have negative signs (Figure 11(f) – (h)), which is the same as the sign of the ICME.

It is noted that deduced axis direction ($\sim 155°$) of the ICME by applying the cylinder fitting model is not consistent with the orientation angle (60°) of the PEA axis, as shown in Figure 11(e). One possible explanation for this disagreement is that the axis of the PEA rotates during propagation from the Sun to the Earth as reported by Cohen *et al.* (2010) and Vourlidas *et al.* (2011).

It is noteworthy that the researchers who participated in CDAW had selected the 17 May CME, not strong but faintly erupted, as the likely candidate of the ICME, because its source region was located close to disk center, while the source location of 16 May CME was far from the disk center. Recently, the 16 May CME was accepted as an alternative candidate for the ICME by CDAW, after the discovery that the eruptive filament near the disk center is related to the arcade formation in AR 10759. Based on our study, we conclude that the solar

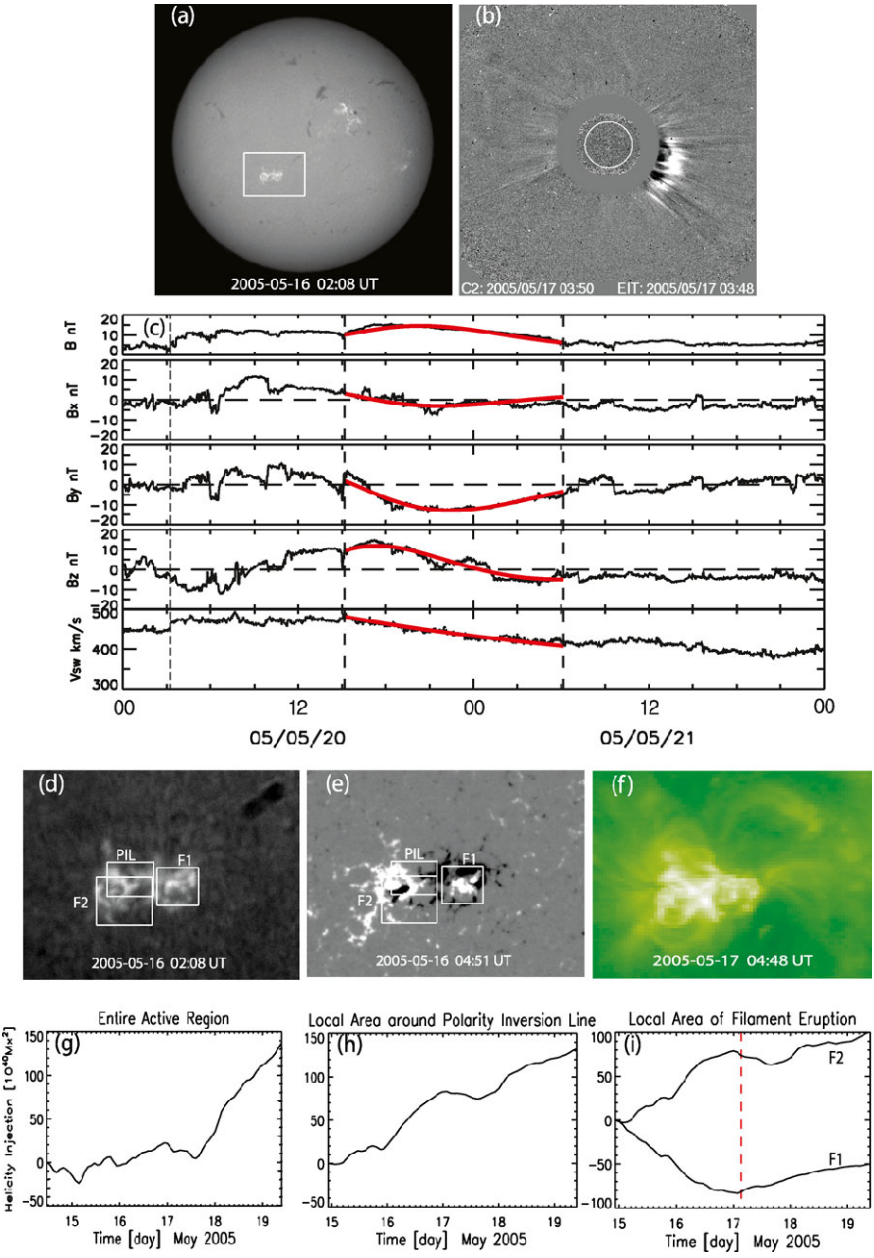


**Figure 10** The 17 May 2005 CME, the possibly associated 20 May 2005 ICME, and their candidate solar source regions. (a) Full disk Yunnan Hα image. The white box denotes the location of AR 10763. (b) LASCO C2 observations of the CME that could produce the ICME observed *in situ* near Earth, shown in (c). Solid red lines denote a fitting result by the cylinder model. The vertical dotted and dashed lines represent the interplanetary shock arrival time and the boundaries of the ICME, respectively. Submaps focusing on AR 9097 prior to the CME eruption are shown in (d) Hα and (e) a magnetogram from SOHO/MDI. (f) Shows SOHO/EIT observations of the same region post-eruption. Estimates of helicity injection in the regions of interest are shown for (g) the entire active region, (h) the polarity inversion line (PIL) and (i) the regions labeled 'F1' and 'F2'. The red dashed vertical line indicates when the flare occurred.

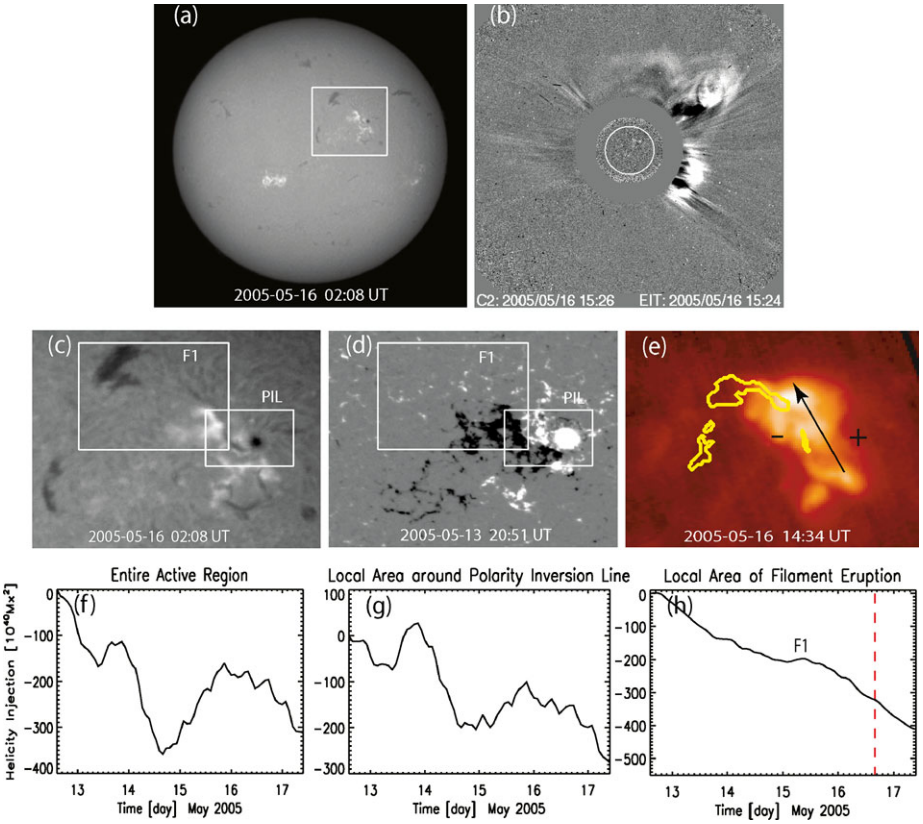


**Figure 11** The 16 May 2005 CME and its potential solar source regions. (a) Full disk Yunnan Hα image. The white box denote the location of AR 10759. (b) LASCO C2 observations of the CME that produced the 20 May 2005 ICME. Submaps focusing on AR 10759 prior to the CME eruption are shown in (c) Hα and (d) a magnetogram from SOHO/MDI. (e) Shows GOES/SXI observations of the same region post-eruption. Estimates of helicity injection in the regions of interest are shown for (f) the entire active region, (g) the polarity inversion line (PIL) and (i) the region labeled 'F1'. The red dashed vertical line indicates when the flare occurred.

source of the 20 May 2005 ICME is more likely to be 16 May 2005 CME, rather than the 17 May 2005 CME.

## 4. Summary and Conclusions

We determined the accumulated amount of helicity injection in the source active regions of CMEs using SOHO/MDI magnetograms, and the helicity sign of the associated ICMEs by fitting the cylinder model developed by Marubashi (2000), assuming a self-similar expansion of the flux rope, to the solar wind data. We confirmed that the helicity signs of ICMEs are generally consistent with that of their solar source regions, in 88 % of the cases. We also compared helicity signs deduced from the X-ray sigmoid shapes with the helicity signs of the ICMEs, and found that about 61 % of the ICMEs have the same helicity signs, while 12 % of the ICMEs have helicity signs that are not in agreement with that of the sigmoid.

However, it was noted that there are many cases (26 %) when the sigmoid's shape is ambiguous in the soft X-ray images. These results indicate that most CMEs contain flux ropes which maintain their helicity signs in the interplanetary space.

By studying four events where the helicity signs differ between the active regions and the ICMEs, we found that the sign inconsistency in two events may be due to one of the following reasons: either incorrect identification of the CME source region (20 May 2005 ICME), or a localised region having a different helicity sign than that of the entire source active region (28 July 2000). The other two events (the 13 – 14 October 2000 ICME and the 20 November 2003 ICME) do not show clear consistency of the sign between the helicity injection through the photosphere and the helicity of the ICMEs. However, we found in both cases that the ICMEs have the same helicity signs as that of the pre-existing coronal magnetic fields in their solar source regions, which were determined by using the LFFF model. These results suggest that the origin of the ICME helicity can be found from the pre-existing magnetic helicity already accumulated in the corona, and the injection of helicity of the opposite sign through the photosphere may result in magnetic reconnection and lead to filament eruptions.

We note that the sigmoid shapes of the source regions of 28 July 2000 and 13 – 14 October 2000 events do indicate a sign of helicity in agreement with the ICME. The sigmoid shape can represent the coronal helicity, opposite to the sign of the photospheric helicity injection. This might illustrate the importance of not relying on a single signature of source region helicity sign when comparing the signs of helicity of CMEs and their associated ICMEs.

In summary, we have found that all ICMEs in this study have the same helicity signs as their solar source regions. Our result reveals that all the CMEs studied in this article have flux rope structure and their helicity signs are conserved while the CMEs propagate from the Sun to the Earth.

**Acknowledgements** We are grateful to the referee for helpful and constructive comments. SOHO is a project of international cooperation between ESA and NASA. We thank the ACE Science center for the ACE data and to the *Yohkoh* SXT team and GOES SXI team for the solar X-ray images. This work benefited from the NASA/LWS Coordinated Data Analysis Workshops on CME flux ropes in 2010 and 2011. We acknowledge the workshop support provided by NASA/LWS, Predictive Science, Inc. (San Diego, CA), University of Alcala (Alcala de Henares, Spain), and Ministerio de Ciencia e Innovacion (Reference number AYA2010-1239-E), Spain. E.-K.L. is supported by AFOSR (FA 9550-12-1-0066). K.-S.C. was supported by the "Development of Korean Space Weather Center" of KASI and the KASI basic research funds.

## References

Alissandrakis, C.E.: 1981, *Astron. Astrophys.* **100**, 197.
Ali, S.S., Uddin, W., Chandra, R., Mary, D.L., Vršnak, B.: 2007, *Solar Phys.* **240**, 89.
Berger, M.A.: 1984, *J. Geophys. Res.* **240**, 89.
Berger, M.A., Field, G.B.: 1984, *J. Fluid Mech.* **147**, 133.
Brueckner, G.E., Howard, R.A., Koomen, M.J., Korendyke, C.M., Michels, D.J., Moses, J.D., Socker, D.G., *et al.*: 1995, *Solar Phys.* **162**, 357.
Burlaga, L., Sittler, E., Mariani, F., Schwenn, R.: 1981, *J. Geophys. Res.* **86**, 6673.
Chae, J.: 2007, *Adv. Space Res.* **39**, 1700.
Chae, J., Sakurai, T.: 2008, *Astrophys. J.* **689**, 593.
Chandra, R., Pariat, E., Schmieder, B., Mandrini, C.J., Uddine, W.: 2010, *Solar Phys.* **261**, 127.
Chen, J.: 1996, *J. Geophys. Res.* **101**, 27499.
Chen, J., Howard, R.A., Brueckner, G.E., Santoro, R., Krall, J., Paswaters, S.E., *et al.*: 1997, *Astrophys. J.* **490**, L191.
Cohen, O., Attrill, G.D.R., Schwadron, N.A., Crooker, N.U., Owens, M.J., Downs, C., Gombosi, T.I.: 2010, *J. Geophys. Res.* **115**, A10104.

Démoulin, P.: 2008, *Ann. Geophys.* **26**, 3113.
Démoulin, P., Mandrini, C.H., van Driel-Gesztelyi, L., Thompson, B.J., Plunkett, S., Kovári, Zs., Aulanier, G., Young, A.: 2002, *Astron. Astrophys.* **382**, 650.
Gosling, J.T., Bame, S.J., McComas, D.J., Phillips, J.L.: 1990, *Geophys. Res. Lett.* **17**, 901.
Gopalswamy, N., Yashiro, S., Michalek, G., Xie, H., Lepping, R.P., Howard, R.A.: 2005, *Geophys. Res. Lett.* **32**, 12.
Gopalswamy, N.: 2006, *Space Sci. Rev.* **124**, 145.
Gopalswamy, N., Yashiro, S., Michalek, G., Stenborg, G., Vourlidas, A., Freeland, S., Howard, R.: 2009, *Earth Moon Planets* **104**, 295.
Gopalswamy, N., Xie, H., Mäkelä, P., Akiyama, S., Yashiro, S., Kaiser, M.K., Howard, R.A., Bougeret, J.-L.: 2010, *Astrophys. J.* **710**, 1111.
Hao, J., Zhang, M.: 2011, *Astrophys. J. Lett.* **733**, L27.
Hu, Q., Dasgupta, B.: 2005, *Geophys. Res. Lett.* **32**, L12109.
Jacobs, C., Roussev, I.I., Lugaz, N., Poedts, S.: 2009, *Astrophys. J. Lett.* **695**, L171.
Jing, J., Park, S.-H., Liu, C., Lee, J., Wiegelmann, T., Xu, Y., Deng, N., Wang, H.: 2012, *Astrophys. J. Lett.* **752**, L9.
Kim, R.-S., Gopalswamy, N., Cho, K.-S., Moon, Y.-J., Yashiro, S.: 2013, *Solar Phys.* doi:10.1007/s11207-013-0230-y
Leamon, R.J., Canfield, R.C., Jones, S.L., Lamdberg, B.J., Pevtsov, A.A.: 2004, *J. Geophys. Res.* **109**, 5106.
Lim, E.-K., Chae, J.: 2009, *Astrophys. J.* **692**, 104.
Lim, E.-K., Jeong, K., Chae, J.: 2007, *Astrophys. J.* **656**, 1167.
Manoharan, P.K., Gopalswamy, N., Yashiro, S., Lara, A., Michalek, G., Howard, R.A.: 2004, *J. Geophys. Res.* **109**, A06109.
Marubashi, K.: 2000, *Adv. Space Res.* **26**, 55.
Marubashi, K., Lepping, R.P.: 2007, *Ann. Geophys.* **25**, 2453.
Marubashi, K., Cho, K.-S., Kim, Y.-H., Park, Y.-D., Park, S.-H.: 2012, *J. Geophys. Res.* **117**, A01101.
Pariat, E., Démoulin, P., Berger, M.A.: 2005, *Astron. Astrophys.* **439**, 1191.
Park, S.-H., Cho, K.-S., Bong, S.-C., Kumar, P., Chae, J., Liu, R., Wang, H.: 2012, *Astrophys. J.* **750**, 48.
Qiu, J., Hu, Q., Howard, T.A., Yurchyshyn, V.B.: 2007, *Astrophys. J.* **659**, 758.
Scherrer, P.H., Bogart, R.S., Bush, R.I., Hoeksema, J.T., Kosovichev, A.G., Schou, J., Rosenberg, W., *et al.*: 1995, *Solar Phys.* **162**, 129.
Schuck, P.W.: 2006, *Astrophys. J.* **646**, 1358.
Smith, C.W., L'Heureux, J., Ness, N.F., Acuña, M.H., Burlaga, L.F., Scheifele, J.: 1998, *Space Sci. Rev.* **86**, 613.
Sung, S.-K., Marubashi, K., Cho, K.-S., Kim, Y.-H., Kim, K.-H., Chae, J., Moon, Y.-J., Kim, I.-H.: 2009, *Astrophys. J.* **699**, 298.
Titov, V.S., Démoulin, P.: 1999, *Astron. Astrophys.* **351**, 707.
Tsuneta, S., Acton, L., Bruner, M., Lemen, J., Brown, W., Caravalho, R., Catura, R.: 1991, *Solar Phys.* **136**, 37.
Vourlidas, A., Colaninno, R., Nieves-Chinchilla, T., Stenborg, G.: 2011, *Astrophys. J. Lett.* **733**, L23.
Yashiro, S., Gopalswamy, N., Michalek, G., St. Cyr, O.C., Plunkett, S.P., Rich, N.B., Howard, R.A.: 2004, *J. Geophys. Res.* **109**, A07105.
Yurchyshyn, V.B., Wang, H., Goode, P.R., Deng, Y.: 2001, *Astrophys. J.* **563**, 381.
Zhang, J., Richardson, I.G., Webb, D.F., Gopalswamy, N., Huttunen, E., Kasper, J., Nitta, N.V.: 2007, *J. Geophys. Res.* **112**, A12103.